Nanoscale duplex oxide growth during early stages of oxidation of Cu-Ni(100)

Guangwen Zhou,[1,*] Dillon D. Fong,[2] Liang Wang,[3,†] Paul H. Fuoss,[2] Peter M. Baldo,[2] Loren J. Thompson,[2] and Jeffrey A. Eastman[2]

[1]*Department of Mechanical Engineering and Multidisciplinary Program in Materials Science and Engineering, State University of New York, Binghamton, New York 13902, USA*

[2]*Materials Science Division, Argonne National Laboratory, Argonne, Illinois 60439, USA*

[3]*Department of Materials Science and Engineering, University of Illinois at Urbana–Champaign, Urbana, Illinois 61801, USA*

(Received 13 August 2009; published 5 October 2009)

A combination of real-time *in situ* synchrotron x-ray diffraction and *ex situ* transmission electron microscopy is utilized to investigate the early stages of oxidation of Cu-Ni(100). Sequential formation of NiO and Cu_2O oxides was observed by increasing oxygen partial pressure, and the Cu_2O phase was identified to form preferentially on top of NiO nanoislands. The origin of this unexpected phenomenon is attributed to localized enrichment of Cu atoms accompanied with NiO growth, which thermodynamically drives the nanoscale Cu_2O/NiO duplex oxide growth.

DOI: 10.1103/PhysRevB.80.134106 PACS number(s): 81.65.Mq, 61.05.C−, 61.82.Bg, 68.37.Lp

I. INTRODUCTION

Understanding the microscopic processes governing initial stages of oxidation of metals has recently been the focus of much research. This interest has been spurred not only by its importance in practical applications such as catalysis, corrosion, and gate oxides, but also by a lack of information on the fundamental processes underlying the initial stages of oxide formation on metal surfaces. Compared to the relatively extensive research on the oxidation of pure metals, the study of early-stage alloy oxidation has been significantly fewer due to the associated complexities, which include different oxygen affinities of the alloying elements, redistribution and segregation of the alloying elements, and the formation of multiple oxide phases and the solid solubility between them.

Early-stage oxidation of unalloyed Cu and Ni has been extensively investigated,[1–6] but little is known regarding the initial reaction of alloyed Cu-Ni with oxygen. Cu and Ni when alloyed form a substitutional solid solution without a miscibility gap but their oxides, Cu_2O and NiO, are immiscible. A comparison of the thermodynamic properties of Cu and Ni using the Ellingham diagram reveals that NiO has a more negative free energy of formation than Cu_2O and, therefore, NiO tends to form more readily than Cu_2O from their respective pure metals.[7] In this case, depending on oxygen partial pressure (pO_2), either one or both components of the alloy will oxidize, thus enabling systematic determination of the effects of compositional and phase evolution during oxidation. In addition to being a model experimental system, understanding the oxidation behavior of Ni-Cu alloys is also of great practical importance because of their wide application such as catalysts[8–10] and corrosion resistance to water environments.[11]

Here we report on the initial oxidation of Cu-Ni(100) surfaces using combined *in situ* synchrotron x-ray scattering and *ex situ* transmission electron microscopy (TEM). We observed sequential formation and reduction in nanosized NiO and Cu_2O oxides by adjusting the pO_2, thereby demonstrating that the relations of free energies (i.e., $\Delta G_{NiO} < \Delta G_{Cu_2O}$) for pure metals hold during the initial oxidation of Cu-Ni alloys. Our *ex situ* TEM observation of oxidized Cu-Ni samples revealed that Cu_2O islands nucleate preferentially on top of NiO islands rather than on bare Cu-Ni surface regions between NiO islands, an intriguing phenomenon defying the expectation based on prevailing knowledge of passivation. Our results demonstrate the importance of oxygen partial pressure in controlling the microstructure of oxide films during alloy oxidation, which have significant technological implications for controlled oxide growth.

II. EXPERIMENTAL DETAILS

The *in situ* synchrotron x-ray scattering experiments were carried out at the Advanced Photon Source, employing a specially designed reaction chamber mounted on an eight-circle diffractometer. The environmental chamber allows the *in situ* study of samples from 300 to 1123 K. Oxidizing and reducing environments are created in the chamber by controlling the pO_2 via mixing purified O_2 and Ar through mass-flow controllers. The samples were 200-nm-thick single-crystalline $(001)Cu_xNi_{1-x}$ films grown on $(001)SrTiO_3$ substrates by electron-beam evaporation. After mounting in the environmental chamber, the samples were annealed at 1123 K for 2 h in an Ar-2% H_2 ambient to produce clean surfaces and then cooled to the desired temperature for study. The films were fully strain relaxed with respect to the $SrTiO_3$ substrate and had a typical mosaic spread of 0.1°. Scattering measurements were performed with 24 keV x rays with a grazing-incidence diffraction geometry. After *in situ* x-ray experiments, the sample was first examined immediately by scanning electron microscopy (SEM) and then by TEM. Cross-sectional TEM specimens were made out of the oxidized/reduced samples using a wedge method,[12] where the oxidized $(001)Cu_xNi_{1-x}$ film was first glued to a Mo ring and a Gatan Precision Ion Polishing System (PIPS) was then used to thin the specimen. The reacted surface was protected by the glue during the PIPS polishing.

III. EXPERIMENTAL RESULTS

Figure 1(a) shows a sequence of in-plane x-ray scans during oxidation of (001)Cu−12.5 at % Ni at T=773 K as a

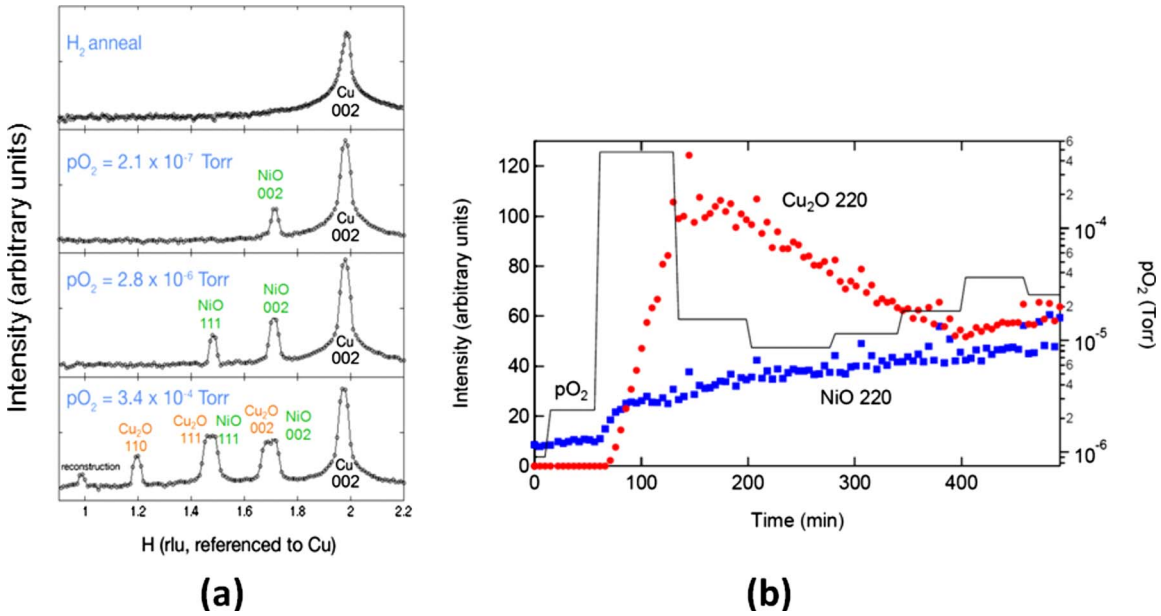

FIG. 1. (Color online) (a) In-plane H00 scans at 773K of the same Cu-Ni(100) surface in varying pO_2 (the H values are shown in reciprocal-lattice units referenced to Cu). Epitaxial NiO forms first when the pO_2 was reached 2.1×10^{-7} Torr. Raising the pO_2 to $\sim1\times10^{-4}$ Torr resulted in oxidation of the Cu component to form Cu_2O nanoislands with multiple orientations; (b) measurements of the integrated intensity of the NiO 220 and Cu_2O 220 Bragg reflections in varying pO_2 revealed that Cu_2O is less stable than NiO, i.e., under $pO_2=9\times10^{-6}$ Torr and $T=773$ K, the NiO islands were stable, while Cu_2O islands underwent reduction.

function of pO_2, where the pO_2 was increased from less than 10^{-10} to $\sim3.4\times10^{-4}$ Torr. The sample exposed to Ar-2% H_2 or low pO_2 environments exhibited the normal diffraction peaks expected for a face-centered cubic copper. Epitaxial NiO started to form first when the pO_2 reached 2.1×10^{-7} Torr, as evidenced by the appearance of the NiO 200 peak. For $pO_2>\sim1\times10^{-4}$ Torr, multiple orientations of Cu_2O are formed. The distinct Cu_2O and NiO peaks are consistent with limited miscibility of Cu_2O and NiO. To compare the thermodynamic stability of NiO and Cu_2O, the intensities of the NiO 220 and Cu_2O 220 reflections were simultaneously monitored while varying the pO_2. Figure 1(b) shows the intensity evolution of NiO 220 and Cu_2O 220 peaks during the oxidation of (001)Cu−9.0 at % Ni at $T=773$ K. The NiO 220 peak is nonzero at $pO_2\geq9.0\times10^{-7}$ Torr, and the intensity never decreases with time, indicating that the equilibrium pO_2 for NiO is less than 9.0×10^{-7} Torr. The intensity of the Cu_2O 220, however, can be made to increase or decrease with varying pO_2, eventually stabilizing at the equilibrium $pO_2\sim2.6\times10^{-5}$ Torr; note that this equilibrium pO_2 is much higher than that predicted for bulk systems, in agreement with the previous study of pure Cu.[6] Therefore, at intermediate pressures (e.g., 9×10^{-6} Torr), Cu_2O islands undergo the reduction reaction, $Cu_2O\rightarrow Cu+O_2$, while NiO islands continue to grow.

In order to obtain a detailed description of the oxide growth, the Cu-Ni sample after the *in situ* x-ray diffraction experiments was further analyzed by *ex situ* TEM. Figure 2(a) is a scanning transmission electron microscopy (STEM) image showing the formation of a NiO island on Cu-Ni(100), it is noted that a small nanoparticle (~10 nm) is formed at the top of the NiO island. Figure 2(b) is from a different area with a much larger NiO island, the island top is covered by a

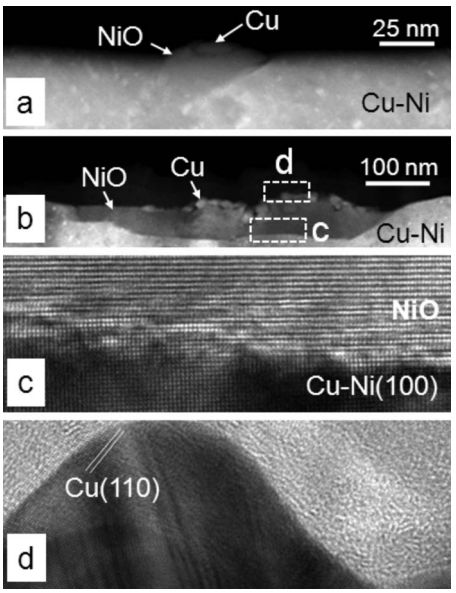

FIG. 2. TEM analysis of the Cu-Ni sample after the reduction in Cu_2O islands. [(a) and (b)] Low-magnification STEM dark field images reveal that Cu nanoparticle nucleate on NiO islands and no Cu nanoparticles are observed on bare Cu-Ni surface area, suggesting that oxidation of the Cu-Ni alloy resulted in nucleation of Cu_2O islands preferentially on NiO islands; (c) HRTEM image from the inner NiO/Cu-Ni interface region marked with the white rectangle c; (d) HRTEM image from the outer interface region indicated by the white rectangle d.

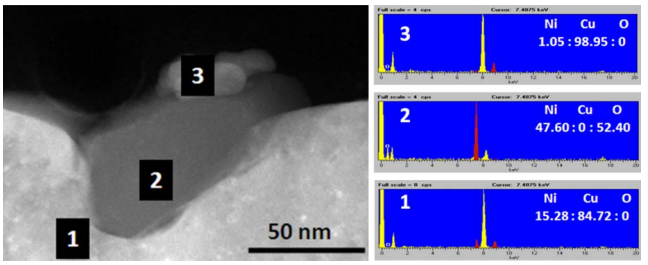

FIG. 3. (Color online) Elemental analysis of the composition of different regions of the Cu-Ni sample. Quantification of the EDS data indicates that region 1 has a Ni/Cu ratio of ~15.28/84.72, and region 2 has a Ni/O ratio of ~47.6/52.4, and region 3 is almost pure Cu.

layer of small nanoparticles. Examination of different sample regions indicates these small nanoparticles are formed preferentially on top of NiO islands, consistent with our SEM observation made immediately after the *in situ* x-ray experiments. Figure 2(c) is a high-resolution (HR) TEM image from the inner interface region as marked by the white rectangle c in Fig. 2(b). The lattice spacing in this region is consistent with NiO structure and the lattice is epitaxial with the underlying Cu-Ni(100) substrate. Figure 2(d) is an HR-TEM image from the outer interface region as marked by the white rectangle d in Fig. 2(b) and the lattice spacing is consistent with Cu{110} planes.

To further confirm the structure analysis, energy dispersive x-ray spectroscopy (EDS) was employed to analyze the chemical composition in different regions of the cross-sectional Cu-Ni TEM specimen. Figure 3(a) shows a dark field STEM image, where the double-layered island structure is visible. STEM-EDS point analyses from three different regions revealed that region 1 contains about 15.28 at % Ni and 84.72 at % Cu, which is close to the original alloy composition; region 2 contains ~47.6 at % Ni and ~52.4 at % O (no Cu is present in this region), which is very close to the stoichiometry of NiO, and region 3 is almost pure Cu.

IV. DISCUSSION

The above TEM analyses reveal that the layer sequence of the reaction product is CuNi/NiO/Cu with Cu being the outermost layer. As known from our *in situ* x-ray scattering experiments [Fig. 1(b)], formation of the outer layer of Cu particles on NiO is due to reduction in original Cu_2O islands that were formed from the oxidation under the higher pO_2 [Fig. 1(a)]. Since reduction in the Cu_2O islands results in new Cu particles either at the original Cu_2O island locations or adjacent regions,[13–17] the product morphology revealed in Figs. 2 and 3 suggests that oxidation of the Cu-Ni alloys under the higher pO_2 leads to formation of Cu_2O nanoislands on top of first-formed NiO islands, rather than on bare Cu-Ni surface regions between NiO islands. According to the theory of metal passivation, such a behavior is quite unexpected because the initially formed NiO islands are supposed to provide protection against further oxidation by preventing direct contact of oxygen gas with the underlying Cu-Ni alloy while the surface of bare Cu-Ni regions between NiO islands

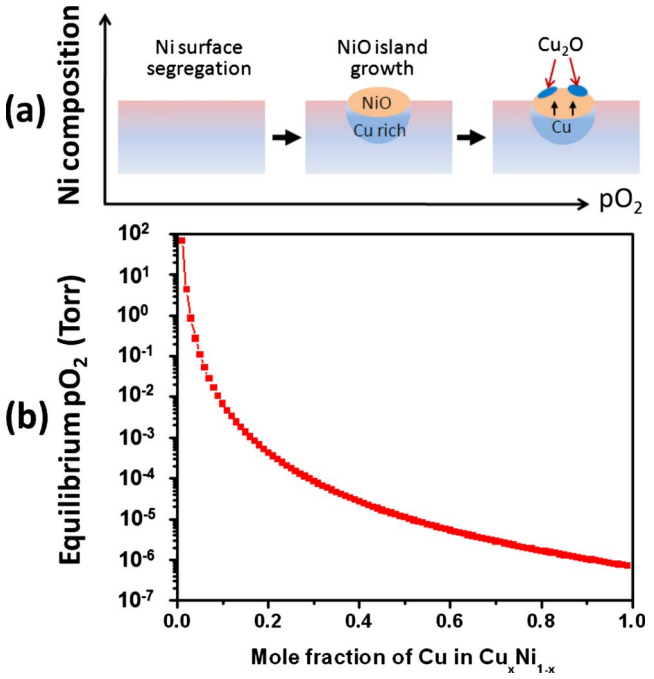

FIG. 4. (Color online) (a) Schematics showing evolution of the surface composition of a Cu-Ni alloy and the duplex Cu_2O/NiO oxide growth as a result of increasing pO_2, where the bare alloy surface regions have an increased content of Ni due to its larger oxygen affinity while the alloy immediately underneath the NiO island has greatly increased Cu composition owing to the localized enrichment of Cu atoms accompanied with the NiO growth; (b) dependence of the equilibrium pO_2 (in logarithm scale) for oxidation of the Cu component on the mole fraction of Cu in the Cu-Ni alloy.

has better contact with oxygen gas and is therefore the expected locations for Cu_2O nucleation.

Since the formation of Cu_2O islands on top of NiO islands requires outward diffusion of Cu atoms through the NiO layer, this seems kinetically unfavorable compared to nucleation of Cu_2O islands on bare Cu-Au alloy surface regions. We therefore first consider the thermodynamic driving force for the Cu_2O formation. As noted in Fig. 1(a), when the Cu-Ni surface was initially oxidized under relatively low pO_2 (e.g., $pO_2 = 2.1 \times 10^{-7}$ Torr), only NiO islands formed. The selective oxidation of Ni in Cu-Ni alloys results in enrichment of Cu atoms on the alloy side of the alloy-oxide interface. On the other hand, due to the larger oxygen affinity of Ni compared to Cu, increasing pO_2 enhances segregation of Ni atoms onto the alloy surface, which was monitored by the total reflection x-ray fluorescence, a technique used in our recent $LaSrMnO_3$ study.[18] The correlation between increasing pO_2 and composition evolution of the alloy surface is schematically shown in Fig. 4(a), where the bare alloy surface has increased Ni composition due to Ni surface segregation while the alloy underneath NiO islands has significantly increased Cu concentration owing to the localized enrichment of Cu atoms accompanied with NiO island growth. Such a behavior of localized enrichment of one of the alloy components accompanied with the oxide growth of the other alloy component has also been observed during our Cu-Au alloy oxidation study.[19,20]

The equilibrium pO_2 for selective oxidation of one component of an alloy depends on the alloy composition. Since Cu and Ni form a solid solution and their oxides are immiscible, the equilibrium pO_2 for Cu oxidation as a function of the alloy composition can be calculated as $pO_2 = \exp(2\Delta G^0_{Cu_2O}/RT - 4 \ln x_{Cu})$, where $\Delta G^0_{Cu_2O} = -130\,930 + 94.5\ T(J/mol)$ is the standard free-energy change for Cu_2O formation, R is the gas constant, T is the oxidation temperature, and x_{Cu} is the mole fraction of Cu in an ideal Cu_xNi_{1-x} solid solution. Figure 4(b) shows the obtained equilibrium pO_2 for Cu oxidation as a function of Cu mole fraction in a Cu-Ni alloy. As can be seen in the plot, increasing Cu mole fraction in the alloy lowers the equilibrium pO_2 for Cu oxidation. We believe this illustrates why Cu atoms underneath NiO islands are preferentially oxidized, leading to the formation of Cu_2O islands on NiO islands. Compared to the alloy composition at bare Cu-Ni surface regions that are enriched with Ni due to Ni surface segregation, the alloy underneath NiO islands has significantly increased Cu content because of the depletion of Ni atoms for NiO growth. Therefore, Cu in the alloy underneath NiO islands has a lower equilibrium pO_2 than that at bare Cu-Ni surface regions and is driven to the outer surface to form Cu_2O nanoislands. Another thermodynamic factor for the preferential nucleation of Cu_2O phase on NiO islands is the reduction in surface energies. The surface energy of NiO [$\gamma_{NiO} \sim 2.6\ J/m^2$ (Ref. 21)] is considerably higher than that of Cu [$\gamma_{Cu} \sim 1.3\ J/m^2$ (Refs. 22 and 23)], Ni [$\gamma_{Ni} \sim 1.6\ J/m^2$ (Refs. 22 and 23)], and Cu_2O [$\gamma_{Cu_2O} \sim 0.8\ J/m^2$ (Ref. 24)], the formation of Cu_2O on NiO is thermodynamically more favorable than on bare alloy surface.

The Cu_2O growth on NiO islands depends also upon kinetic factors. Cu_2O and NiO are both metal-deficient oxides and the predominant point defects are metal vacancies.[25,26] Metal diffusion is several orders of magnitude faster than oxygen in both oxides.[27–29] The growth of Cu_2O on NiO islands is facilitated by outward diffusion of Cu ions through the NiO layer via these metal vacancies. This explains why Cu_2O phase is formed on top of NiO islands rather than at the inner NiO-alloy interface. The reason why the localized enrichment of Cu is not seen in the composition shown in Fig. 3 is because the Cu has already migrated to the top. Meanwhile, as noted from Figs. 2 and 3, the surface morphology of NiO islands is not well defined and different orientations of Cu_2O islands can be nucleated on NiO islands. This is consistent with Fig. 1(a), where the formation of multiple orientations of Cu_2O was observed.

The observed duplex oxide growth may have significant implications for controlling the microstructure of oxide films during alloy oxidation. For instance, by manipulating pO_2, a double-layered oxide structure consisting of an outer layer of copper oxide and an inner NiO layer can be grown by suppressing nucleation of Cu_2O islands on the bare Cu-Ni surface. This duplex oxide structure is expected to hold better protection properties than the oxides formed under high pO_2, where an inner porous layer consisting of a mixture of Cu_2O and NiO particles is often observed.[26,30] The formation of the inner porous oxide layer can be attributed to the poor coalescence between NiO and Cu_2O islands that are simultaneously nucleated on the bare Cu-Ni surface because of the high pO_2. On the other hand, our experimental finding reported here may also inspire new research and experiments in this topic, such as *in situ* environmental TEM that could follow directly (and reversibly) the duplex oxide growth at the atomic scale.

V. CONCLUSIONS

In conclusion, we have shown that the initial oxidation of Cu-Ni alloys under controlled pO_2 results in double-layered Cu_2O/NiO nanoisland growth. This nanoscale duplex oxide growth is thermodynamically driven by localized Cu enrichment in the Cu-Ni alloy immediately underneath growing NiO islands, which lowers the equilibrium pO_2 for oxidation of the Cu component in the alloy. We expect that this phenomenon of nanoscale duplex oxide growth holds generally because the metal elements in most alloy systems exhibit different oxygen affinities. The results here show the importance of oxygen partial pressure in controlling the microstructure of oxide films during the oxidation of alloys.

ACKNOWLEDGMENTS

The authors thank the APS sector 12 (BESSRC) staff for their assistance. Guangwen Zhou gratefully acknowledges support from the National Science Foundation (NSF) under the Grant No. CMMI-0825737. Work performed at Argonne National Laboratory was supported by UChicago Argonne, LLC, Operator of Argonne National Laboratory. Argonne, a U.S. Department of Energy Office of Science Laboratory, is operated under Contract No. DE-AC02-06CH11357.

*Corresponding author; gzhou@binghamton.edu

†Present address: Texas Instruments, 12500 TI Boulevard, Dallas, TX 75243, USA.

[1] R. H. Milne and A. Howie, Philos. Mag. A **49**, 665 (1984).

[2] P. H. Holloway and J. B. Hudson, Surf. Sci. **43**, 123 (1974).

[3] J. C. Yang, D. Evan, and L. Tropia, Appl. Phys. Lett. **81**, 241 (2002).

[4] G. W. Zhou and J. C. Yang, Phys. Rev. Lett. **89**, 106101 (2002).

[5] G. W. Zhou, W. S. Slaughter, and J. C. Yang, Phys. Rev. Lett. **94**, 246101 (2005).

[6] J. A. Eastman, P. H. Fuss, L. E. Rehn, P. M. Baldo, G. W. Zhou, D. D. Fong, and L. J. Thompson, Appl. Phys. Lett. **87**, 051914 (2005).

[7] O. Kubaschewski and C. B. Alcock, *Metallurgical Thermochemistry* (Pergamon, Oxford, 1979).

[8] P. J. Durham, R. G. Jordan, G. S. Sohal, and L. T. Wille, Phys. Rev. Lett. **53**, 2038 (1984).

[9] W. F. Egelhoff, Jr., Phys. Rev. Lett. **50**, 587 (1983).

[10] V. Kumar, Phys. Rev. B **23**, 3756 (1981).
[11] K. Hono, M. Nakamura, and H. W. Pickering, Surf. Sci. **245**, 132 (1991).
[12] P. M. Voyles, J. L. Grazul, and D. A. Muller, Ultramicroscopy **96**, 251 (2003).
[13] J. A. Rodriguez, J. C. Hanson, A. I. Frenkel, J. Y. Kim, and M. Perez, J. Am. Chem. Soc. **124**, 346 (2002).
[14] J. Y. Kim, J. A. Rodriguez, J. C. Hanson, A. I. Frenkel, and P. L. Lee, J. Am. Chem. Soc. **125**, 10684 (2003).
[15] G. W. Zhou, W. Dai, and J. C. Yang, Phys. Rev. B **77**, 245427 (2008).
[16] G. W. Zhou and J. C. Yang, Phys. Rev. Lett. **93**, 226101 (2004).
[17] C. H. Bamford, C. F. H. Tipper, and R. G. Compton, *Comprehensive Chemical Kinetics* (Elsevier, New York, 1984), Vol. 21.
[18] T. T. Fister, D. D. Fong, J. A. Eastman, P. M. Baldo, M. J. Highland, P. H. Fuoss, K. R. Balasubramaniam, J. C. Meador, and P. A. Salvador, Appl. Phys. Lett. **93**, 151904 (2008).
[19] G. W. Zhou, L. Wang, R. C. Birtcher, P. M. Baldo, J. E. Pearson, J. C. Yang, and J. A. Eastman, Phys. Rev. Lett. **96**, 226108 (2006).
[20] G. W. Zhou, J. A. Eastman, R. C. Birtcher, P. M. Baldo, J. E. Pearson, L. J. Thompson, L. Wang, and J. C. Yang, J. Appl. Phys. **101**, 033521 (2007).
[21] A. Wander, I. J. Bush, and N. M. Harrison, Phys. Rev. B **68**, 233405 (2003).
[22] S. M. Foiles, M. I. Baskes, and M. S. Daw, Phys. Rev. B **33**, 7983 (1986).
[23] Y. N. Wen and J. M. Zhang, Solid State Commun. **144**, 163 (2007).
[24] A. Soon, M. Todorova, B. Delley, and C. Stampfl, Phys. Rev. B **75**, 125420 (2007).
[25] P. Kofstad, *High Temperature Corrosion* (Elsevier Applied Science, New York, 1988).
[26] R. Haugsrud and P. Kofstad, Oxid. Met. **50**, 189 (1998).
[27] S. Mrowec, A. Stoklosa, and K. Godlewski, Cryst. Lattice Defects **5**, 239 (1974).
[28] A. Atkinson and R. I. Taylor, Philos. Mag. A **39**, 581 (1979).
[29] H. Inaba, J. Mater. Sci. **32**, 91 (1997).
[30] R. Haugsrud, Corros. Sci. **42**, 383 (2000); Oxid. Met. **53**, 427 (1999).